



PERGAMON

Available online at www.sciencedirect.com

SCIENCE @ DIRECT®

Scripta Materialia 49 (2003) 997–1002



www.actamat-journals.com

Deformation behavior of stainless steel particles under compressive load

H. Hashimoto^{*}, Z.M. Sun, T. Abe

*Institute for Structural and Engineering Materials, National Institute of Advanced Industrial Science and Technology (AIST),
4-2-1, Nigatake, Miyagino-ku, Sendai 983-8551, Japan*

Received 9 May 2003; received in revised form 26 June 2003; accepted 5 August 2003

Abstract

Spherical stainless steel particles with diameters of 0.040–0.185 mm plastically deform immediately on compressive loading. The load–displacement relationship was observed to be approximately linear in the range of displacement within 5% of the particle size.

© 2003 Acta Materialia Inc. Published by Elsevier Ltd. All rights reserved.

Keywords: Powder consolidation; Steels; Plastic deformation; Yield phenomena

1. Introduction

Die-compaction of metal powders, for the purpose of densification and shape forming, is one of the most important processes in the powder metallurgical industry. Our main interest is in the density of compacted powders, which affects the shrinkage of compacted powders during sintering and in turn the dimensional precision and strength of sintered compacts. To describe powder densification behavior during die-compaction, many theoretical, semi-theoretical and empirical compaction equations have been proposed [1], most of which express the correlation between the average density of compacted powders and compacting

pressure. These equations are useful for predicting the density of compacted powders for simple shapes formed by conventional die-compaction, in which only a narrow density distribution is seen. Recent developments in computer numerical control (CNC) pressing technology, however, have enabled the die-compaction of compacts with very complex shapes. In general, compacted powders of complicated shapes show wide density distributions, making conventional compaction equations inapplicable. As a result, the dimensions and the shapes of the press dies as well as of the processing conditions have up to now been optimized by trial and error, since the density of compacts affects shrinkage and dimensional precision.

Due to recent developments in computer technology, model simulation of the powder densification behavior during die-compaction is able to offer a practical means of predicting powder density distributions. Extensive work has been reported on the successful prediction of density

^{*} Corresponding author. Tel.: +81-222-375-216; fax: +81-223-366-839.

E-mail address: hitoshi-hashimoto@aist.go.jp (H. Hashimoto).

distributions by simulating powder densification behavior using the finite element method (FEM) [2–5]. However, the FEM simulation is based on the assumption that the compacted powder is a continuous medium. Consequently, FEM simulation is not the most appropriate technique at the early stages of compaction in which the powder particles are not yet ‘cold-welded’ with each other and move into the large voids present in the powder, which results in densification of the powder by a simple change of particle distribution. This phenomenon is called particle rearrangement. The FEM method is, moreover, not appropriate in cases where particles need to travel long distances, such as in a complex die set, during the process of CNC pressing.

In the particle rearrangement stage, model simulation based on the discrete element method (DEM) [6] enables the description of powder densification behavior. The principle of the DEM simulation is the successive solution of equations of motion for individual particles. Therefore, forces acting on contact areas between particles and between die walls and particles need to be taken account of in equations of motion for the individual particles in the DEM simulation. These contact forces consist of elastic repulsion, plastic deformation resistance and frictional resistance. To obtain more reliable results by DEM simulation, these contact forces need to be estimated precisely. Either the elastic repulsion or the plastic deformation resistance can be divided into two components: the normal component and the tangential component, which act in the normal and tangential directions to the contact surface. The tangential component does not exceed the frictional resistance, because particles in contact start to slip when the tangential component is greater than the frictional resistance. On the other hand, the frictional resistance is given by the product of frictional coefficient and the normal component; hence, of all the forces and components, the normal

components of elastic repulsion and the plastic deformation resistance are the parameters that need to be the most precisely estimated in a DEM simulation.

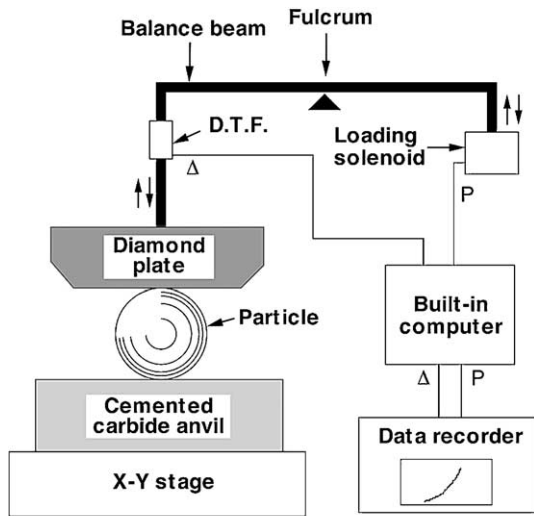
In this study, single particles of stainless steel in a size range from 0.040 to 0.185 mm were compressed between parallel plates using a micro-loading apparatus. The compressive load and displacement in the loading direction were measured to obtain the relation of the normal components of elastic repulsion and plastic deformation resistance to the deformation of the particles.

2. Experimental

Spherical particles (particle size range: 0.040–0.185 mm) of 316L-type stainless steel (designated as SUS316L in Japan), produced by a plasma rotating electrode centrifugal atomization method, were subjected to compression testing. The chemical composition of SUS316L is listed in Table 1. The test was conducted by means of a special micro-loading apparatus that was obtained by modifying a dynamic micro-hardness tester. An outline of the micro-loading apparatus is shown in Fig. 1. A diamond loading plate (size of plane area 0.5 mm×0.5 mm) was fixed to a rod connected to the end of a balance beam. At the other end of the beam, a solenoid was installed to drive the beam end up and down for loading and unloading. A built-in computer was used to control the load and loading rate by regulating the electric current applied to the solenoid. One particle was put on an anvil made of cemented carbide (16 mm×16 mm×4 mm) and anchored using a small amount of soft resin. The anvil was fixed firmly to the X–Y stage of the loading apparatus. The particle was centered on the loading plate. The particle was then compressed at a constant loading rate (0.00627 N/s). The maximum compressive load

Table 1
Chemical composition of SUS316L

Ni	Cr	Mo	Mn	P	Si	C	S	Fe
12.09	16.26	2.01	1.69	0.035	0.025	0.013	0.011	Balance



D.T.F.: Differential transformer

Fig. 1. Schematic illustration of micro-loading apparatus.

was 0.98 N. The compressive load was calculated from the electric current applied to the solenoid by the built-in computer. The displacement in the loading direction was measured by a differential transformer fixed to the rod connecting the diamond plate to the end of the balance beam. The experimental resolutions were 0.49 mN for the load and 0.02 μm for the displacement. A digital data recorder was used to record the load and the displacement at a sampling rate of 0.2 s. Before and after the test, the particle was observed and photographed using an optical microscope with a digital camera and a scanning electron microscope. The particle size was measured on the photograph.

3. Results and discussion

SEM images of a 0.102 mm 316L particle before and after compression up to 0.98 N are shown in Fig. 2(a) and (b), respectively. It is obvious that a plane surface was formed due to plastic deformation of the particle during compression. To consider the yielding behavior of the particle, the experimental load–displacement relation was compared with predictions based on elastic theory. The theoretical relation for an elastic sphere made of 316L compressed between the diamond plate and the cemented carbide anvil is given by the following equation derived from Hertz contact theory [7]

$$\Delta = \frac{1}{2} 3^{2/3} d^{-1/3} \left[\left(\frac{1 - \nu_1^2}{E_1} + \frac{1 - \nu_2^2}{E_2} \right)^{-2/3} + \left(\frac{1 - \nu_1^2}{E_1} + \frac{1 - \nu_3^2}{E_3} \right)^{-2/3} \right] P^{2/3}, \quad (1)$$

where P [N] is the compressive load, Δ [m] the displacement in the loading direction, d [m] the diameter of the 316L particle, E_1 [Pa] and ν_1 elastic modulus and Poisson's ratio of the 316L particle, respectively, E_2 [Pa] and ν_2 those of the diamond plate, and E_3 [Pa] and ν_3 those of the cemented carbide anvil. The elastic moduli and Poisson's ratios of these materials [8–10] are listed in Table 2. Fig. 3 shows a load–displacement curve measured for the 0.102 mm 316L particle and a corresponding theoretical curve calculated from Eq. (1). The experimental curve (except in the early stages of loading) yields much larger strains for a

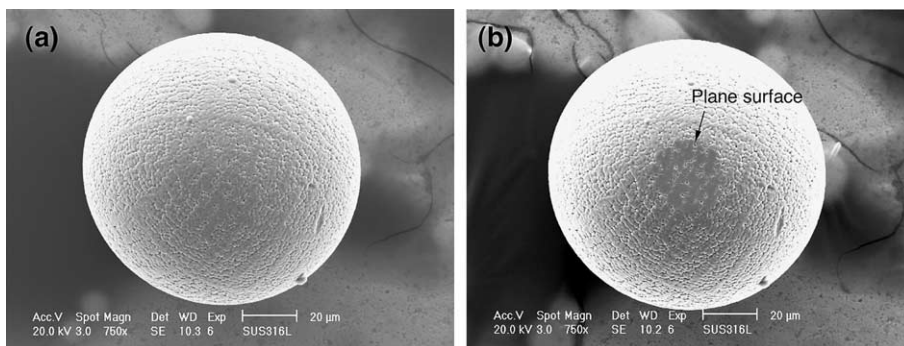


Fig. 2. SEM images of 316L particle (a) before and (b) after compression test.

Table 2
Elastic moduli and Poisson's ratios of SUS316 [8], diamond [9] and cemented carbide [10]

Material	Elastic modulus E [GPa]	Poisson's ratio ν
SUS316	191–196	0.23
Diamond	1220	0.20
Cemented carbide	593	0.21

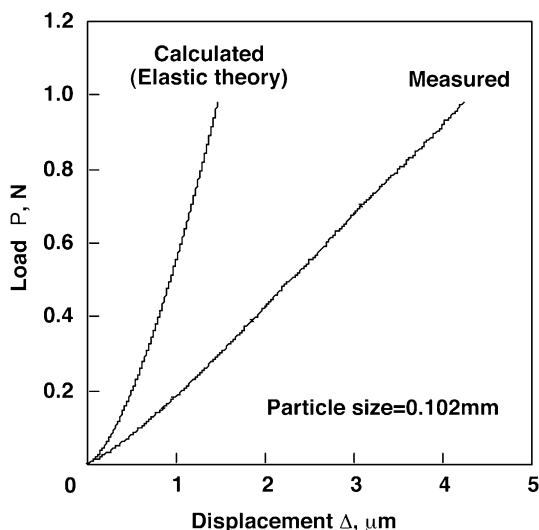


Fig. 3. Load–displacement curve measured for a 0.1020-mm 316L particle compressed up to 0.98 N.

given load than predicted by elastic theory. It can be understood from Fig. 3 that the 316L particle yielded at a quite low compressive load. This result could be also confirmed by comparison with predictions based on plastic theory using FEM simulation approach [11].

Fig. 4 shows typical load–displacement curves measured for various sizes of 316L particles compressed up to 0.98 N. The displacement is shown as the normalized displacement (displacement divided by particle size). In the range of normalized displacements up to 5%, the curves can be approximated by straight lines. However, the curves bend abruptly in the range between 5% and 10% and exhibit significantly shallower slopes in the range over 10%. In other words, the particles show abnormal deformation behavior in the displacement range above 10% of the particle size. Fig. 5(a)

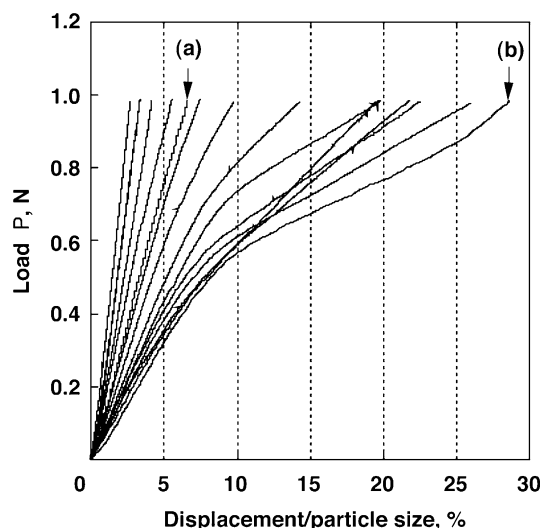


Fig. 4. Variety of load–displacement curves measured for 316L particles compressed until 0.98 N.

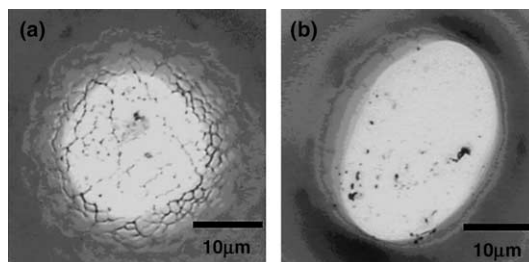


Fig. 5. Optical micrographs of 316L particle after compression test; (a) and (b) correspond with those in Fig. 4.

and (b) show optical micrographs of 316L particles after the compression test. The load–displacement curves of these particles are already shown in Fig. 4. Letters (a) and (b) in Fig. 4 correspond to the same letters indicated in Fig. 5, respectively. Namely, the letter (a) indicates that the particle deformed within 10% and the letter (b) the particle deformed to more than 10% of the particle size. Plane surfaces formed by plastic deformation are seen in both particles. Fig. 5(a) shows a circular plane surface, while (b) shows an elliptical one. Both particles were confirmed to be almost spherical by optical microscopy before compression. Therefore, the elliptical plane surface in Fig. 5(b) was formed by squeezing the particles. This

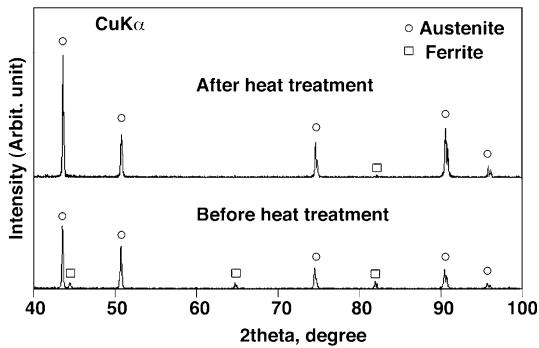


Fig. 6. X-ray diffraction patterns of 316L particles before and after heat treatment.

inhomogeneous deformation may have caused the abnormal load–deformation relations shown in Fig. 4.

Fig. 6 shows X-ray diffraction patterns of the particles. The particles show peaks from ferrite as well as austenite, in the pattern indicated as before heat treatment. According to Bouche et al. [12], δ -ferrite dendrites were found in a matrix of γ columnar grains in 316L weldments. Therefore, the two-phase (ferrite and austenite) structure of the 316L particles was presumably caused by rapid cooling of droplets of 316L melt during the atomization process. The rapid cooling of droplets is presumed to cause a difference in cooling rate, and therefore solidification rate, between the surface and the core part of the particle, due to the poor thermal conductivity of 316L; this results in particles comprising a soft core covered with a hard crust. We assume that the plastic deformation took place within the hard crust in the range of displacement of less than 5% of the particle size, while in the displacement range over 10%, the plastic deformation reached the soft core and the overall plastic deformation behavior became more complex. The cause of elliptical surfaces formation can be understood as follows. During plasma rotating electrode centrifugal atomization process, droplets of 316L melt flew in an inert gas and were cooled by gas flow around the droplets. Since the flow speed of gas at the surface of droplets was inhomogeneous, cooling rate was inhomogeneous over the surface. It is easily understood that the flow speed is the fastest at ‘equator’ of the spherical

droplets if the gas flows from ‘north pole’ to ‘south pole’. Therefore, the hard crust becomes thicker at the ‘equator’ than at the ‘poles’. Such 316L spherical particles consisting of the soft core covered with inhomogeneous hard crust deformed inhomogeneously and formed the elliptical plain surfaces. According to Kobayashi et al. [13], the δ -ferrite in 25Cr–7Ni–0.14N stainless steel decomposes into austenite and chromium nitride at temperatures over 823 K. Therefore, heat treatment of the particles at 1118 K for 1.8 ks in a vacuum was conducted to decompose the ferrite. An XRD pattern of the particles after heat treatment is also shown in Fig. 6. Compared with the pattern of the particles before treatment, the intensity of peaks from ferrite was reduced in the heat-treated particles. Typical load–displacement curves of the heat-treated particles are shown with those of the untreated ones in Fig. 7. It is evident from the figure that the abnormal load–displacement relationship was corrected by the heat treatment, which supports our above-mentioned hypothesis.

Finally, the particles in the size range from 0.040 to 0.185 mm were tested, and the slope of the approximated lines for load–displacement relation in the range of displacement less than 5% of the particle size was calculated using the mean square

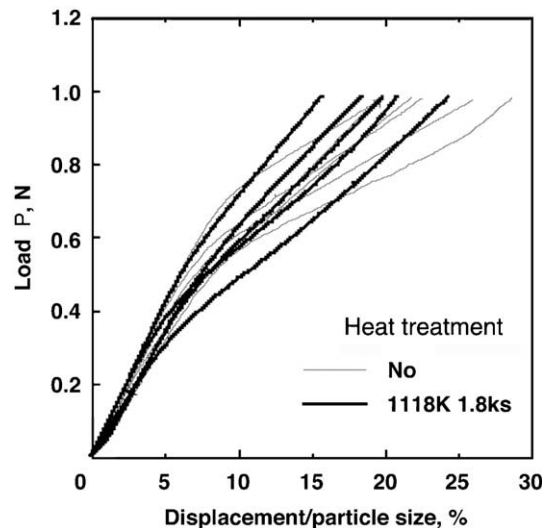


Fig. 7. Effect of heat treatment on load–displacement relation.

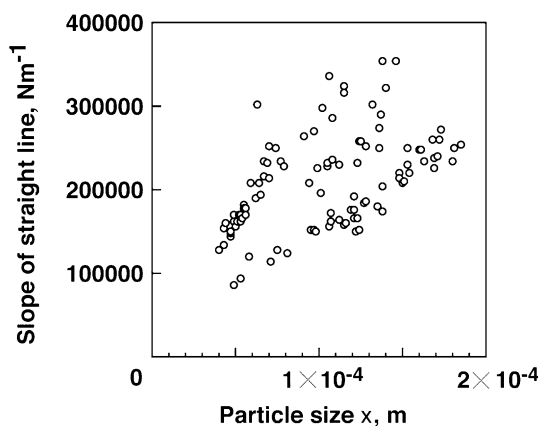


Fig. 8. Correlation between particle size and slope of approximated line for load–displacement relation.

fitting method and plotted against the particle size in Fig. 8. Although the slope tends to increase with an increase in particle size, the plotted data spread so widely that no clear correlation between the slope and particle size could be established.

4. Conclusions

The deformation behavior of small stainless steel (316L) particles in the size range from 0.040 to 0.185 mm under compressive load was investigated using a micro-loading apparatus. The following were obtained as our conclusions: (1) The particles started to deform plastically immediately after the start of loading. (2) The load–displacement relationship is approximately a straight line in the range of displacement up to 5% of the particle size. (3) The slope of the load–displace-

ment curve becomes shallower in the range of displacement over 10% of the particle size due to inhomogeneous deformation of the particles, which consist of a hard crust around a soft core.

Acknowledgements

The authors express special thanks to Prof. F. Saito (Institute of Multidisciplinary Research for Advanced Materials, Tohoku University) and Dr. M. Nishida (Fukuda Metal Foil & Powder Co., Ltd.) for their kind help with preparation of the compression test.

References

- [1] Denny PJ. Powder Technol 2002;127:162.
- [2] Haeggblad HA. Powder Technol 1991;67:127.
- [3] Gethin DT, Tran VD, Lewis RW, Arrifin AK. Int J Powder Metall 1994;30:385.
- [4] Kraft T, Riedel H, Stingel P, Wittig F. Adv Eng Mater 1999;1:107.
- [5] Coube O, Riedel H. Powder Metall 2000;43:123.
- [6] Cundall PA, Strack ODL. Geotechnique 1979;29:47.
- [7] Timoshenko SP, Goodier JN. Theory of elasticity. 3rd ed. Tokyo: McGraw-Hill Kogakusha Ltd; 1970. p. 409.
- [8] The Japan Society of Mechanical Engineers. The modulus of elasticity of metals and alloys. Tokyo: JSME; 1980. p. 99.
- [9] Spear KE, Dismukes JP. Synthetic diamond. Emerging CVD science and technology. New York: Wiley; 1994. p. 4.
- [10] Saito F. Doctoral thesis of Tohoku University. 1982. p. 15.
- [11] Mesarovic SD, Fleck NA. Int J Solid Struct 2000;37:7071.
- [12] Bouche G, Bechade JL, Mathon MH, Allais L, Gourgues AF, Naze L. J Nucl Mater 2000;277:91.
- [13] Kobayashi S, Nakai K, Ohmori Y. Acta Mater 2001;49:1891.